JCI The Journal of Clinical Investigation

Whole-brain circuit dissection in free-moving animals reveals cell-specific mesocorticolimbic networks

Michael Michaelides, … , Nora D. Volkow, Yasmin L. Hurd

J Clin Invest. 2013;123(12):5342-5350. https://doi.org/10.1172/JCI72117.

Technical Advance

The ability to map the functional connectivity of discrete cell types in the intact mammalian brain during behavior is crucial for advancing our understanding of brain function in normal and disease states. We combined designer receptor exclusively activated by designer drug (DREADD) technology and behavioral imaging with μPET and [^{18}F]fluorodeoxyglucose (FDG) to generate whole-brain metabolic maps of cell-specific functional circuits during the awake, freely moving state. We have termed this approach DREADD-assisted metabolic mapping (DREAMM) and documented its ability in rats to map whole-brain functional anatomy. We applied this strategy to evaluating changes in the brain associated with inhibition of prodynorphin-expressing (*Pdyn*-expressing) and of proenkephalin-expressing (*Penk*-expressing) medium spiny neurons (MSNs) of the nucleus accumbens shell (NAcSh), which have been implicated in neuropsychiatric disorders. DREAMM revealed discrete behavioral manifestations and concurrent engagement of distinct corticolimbic networks associated with dysregulation of *Pdyn* and *Penk* in MSNs of the NAcSh. Furthermore, distinct neuronal networks were recruited in awake versus anesthetized conditions. These data demonstrate that DREAMM is a highly sensitive, molecular, high-resolution quantitative imaging approach.

Whole-brain circuit dissection in free-moving animals reveals cell-specific mesocorticolimbic networks

Michael Michaelides,[1,2] Sarah Ann R. Anderson,[1,2] Mala Ananth,[3] Denis Smirnov,[4] Panayotis K. Thanos,[3,5] John F. Neumaier,[4] Gene-Jack Wang,[1,3] Nora D. Volkow,[5] and Yasmin L. Hurd[1,2,6]

[1]Department of Psychiatry and [2]Department of Neuroscience, Friedman Brain Institute, Icahn School of Medicine at Mount Sinai, New York, New York, USA. [3]Biosciences Department, Brookhaven National Laboratory, Upton, New York, USA. [4]Psychiatry and Behavioral Sciences and Pharmacology, University of Washington, Seattle, Washington, USA. [5]Laboratory of Neuroimaging, National Institute on Alcohol Abuse and Alcoholism, Bethesda, Maryland, USA. [6]James J. Peters VA Medical Center, New York, New York, USA.

The ability to map the functional connectivity of discrete cell types in the intact mammalian brain during behavior is crucial for advancing our understanding of brain function in normal and disease states. We combined designer receptor exclusively activated by designer drug (DREADD) technology and behavioral imaging with μPET and [^{18}F]fluorodeoxyglucose (FDG) to generate whole-brain metabolic maps of cell-specific functional circuits during the awake, freely moving state. We have termed this approach DREADD-assisted metabolic mapping (DREAMM) and documented its ability in rats to map whole-brain functional anatomy. We applied this strategy to evaluating changes in the brain associated with inhibition of prodynorphin-expressing (*Pdyn*-expressing) and of proenkephalin-expressing (*Penk*-expressing) medium spiny neurons (MSNs) of the nucleus accumbens shell (NAcSh), which have been implicated in neuropsychiatric disorders. DREAMM revealed discrete behavioral manifestations and concurrent engagement of distinct corticolimbic networks associated with dysregulation of *Pdyn* and *Penk* in MSNs of the NAcSh. Furthermore, distinct neuronal networks were recruited in awake versus anesthetized conditions. These data demonstrate that DREAMM is a highly sensitive, molecular, high-resolution quantitative imaging approach.

Introduction

The mammalian brain is a complex organ with billions of heterogeneous cells whose local and long-range functional connections regulate behavior and physiology. Traditional approaches used for mapping functional brain anatomy do not provide information on long-range, global (i.e., intact whole brain) circuits. Recently, optogenetics was coupled with in vivo functional MRI (fMRI) and allowed, for what we believe is the first time, assessment of functional anatomy of discrete cell types in living animals (1, 2). fMRI technology, however, relies on nonmolecular, indirect measures of neuronal activity (i.e., neurovascular coupling) and is limited in its applicability to anesthetized or immobilized animals. Importantly, a recent study showed that light delivery in the absence of optogenetic stimulation induced strong local fMRI responses in the stimulated site (3). To overcome these limitations, we combined designer receptor exclusively activated by designer drug (DREADD) technology (4), which allows remote in vivo control of cell-specific firing (5), together with behavioral imaging using μPET and [^{18}F]fluorodeoxyglucose (FDG) to measure regional brain glucose metabolism, which is a direct marker of brain function (6–9). This approach, termed DREADD-assisted metabolic mapping (DREAMM), was used to map functional brain anatomy associated with inhibiting the activity of prodynorphin-expressing (*Pdyn*-expressing) and of proenkephalin-expressing (*Penk*-expressing) medium spiny neurons (MSNs) in the medial nucleus accumbens shell (NAcSh), highly implicated in neuropsychiatric disorders. *Pdyn*-expressing MSNs in the NAcSh, which comprise the "direct" (Go) output pathway, send direct inhibitory projections to the ventral tegmental area (VTA) and substantia nigra pars reticulata (SNr) as well as inhibitory projections to the medial ventral pallidum (VPm) (10). In contrast, NAcSh *Penk*–expressing MSNs, which comprise the "indirect" (NoGo) output pathway, send inhibitory projections predominantly to the VPm (10). The "direct" and "indirect" NAc pathways exert effects on behaviors and emotions dysregulated in addiction and other psychiatric illnesses, but the global circuits linked to these specific pathways are unknown. We examined the capacity of DREAMM to provide in vivo information regarding the direct anatomical connectivity of *Pdyn*- or *Penk*-expressing MSNs as well as the time-dependent response of downstream circuits recruited after inhibition of each MSN subtype. Moreover, we evaluated DREAMM during awake FDG uptake in freely moving rats to assess behaviorally relevant functional connectivity specific to altering the activity of each MSN.

Results

Given the novel nature of the technique, we first wanted to validate the temporal sensitivity by examining time-dependent brain activity changes in a well-characterized neuronal circuit that could be directly studied in relation to exogenous stimulation. Therefore, we used the well-established vibrissae stimulation model, which is known to activate the barrel field somatosensory cortex (11). We scanned naive adult (P55-P69) male Sprague Dawley (SD) rats (n = 6) using a dynamic scanning procedure in which anesthe-

Conflict of interest: The authors have declared that no conflict of interest exists.
Citation for this article: *J Clin Invest.* 2013;123(12):5342–5350. doi:10.1172/JCI72117.

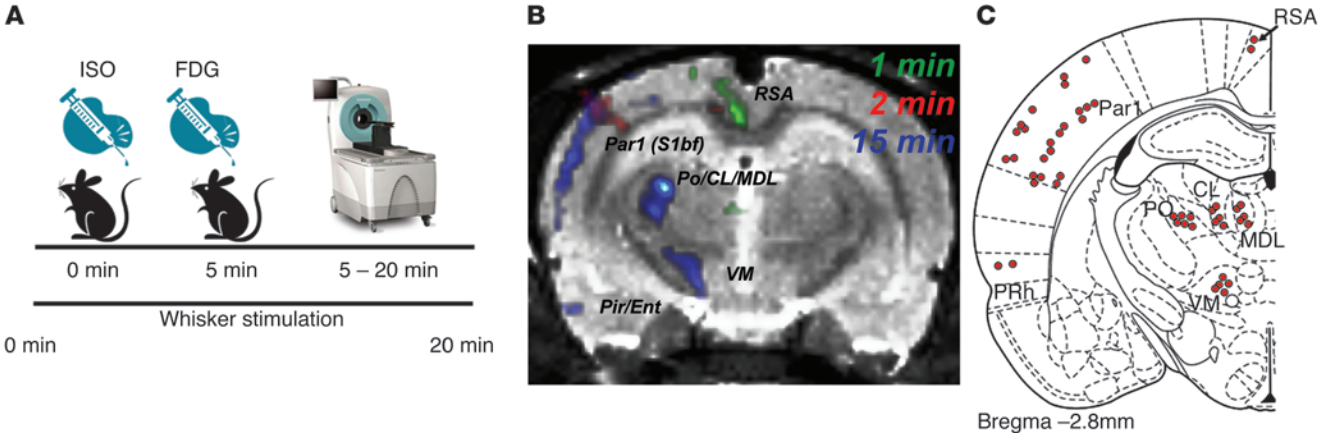

Figure 1
Vibrissae stimulation leads to time-dependent brain activation in barrel field circuitry. (**A**) μPET imaging protocol. Rats were anesthetized with isoflurane (ISO) and placed on the scanner bed; unilateral vibrissae stimulation was initiated. Five minutes later, rats were injected i.v. with approximately 0.6 mCi of FDG and scanning commenced. Stimulation lasted for 15 minutes. (**B**) Time-dependent increases in contralateral FDG uptake in response to unilateral vibrissae stimulation; (**C**) afferent and efferent connectivity of the vibrissal MC. Par1, parietal cortex; S1bf, primary somatosensory cortex barrel field; RSA, agranular retrosplenial cortex; Po, posterolateral thalamus; CL, centrolateral thalamus; MDL, lateral part of mediodorsal thalamus; VPL, lateral part of ventroposterior thalamus; VM, ventromedial thalamus; PRh, perirhinal cortex. Adapted with permission from *Experimental Brain Research* (11).

tized rats were subjected to continuous unilateral vibrissae stimulation that was initiated 5 minutes prior to intravenous i.v. FDG injection. Scans were then normalized to Paxinos stereotaxic coordinates (12) and analyzed using statistical parametric mapping (SPM) as previously described (7). Using this dynamic approach, we observed time-dependent contralateral barrel field circuit activation as early as 1 minute after FDG injection (Figure 1). The anatomical specificity of this activation directly overlapped known connectivity of the barrel field circuit (ref. 11 and Figure 1), exemplifying the sensitivity of our imaging methodology in detecting functional changes in brain activity with significant anatomical and temporal specificity (single-minute resolution). To our knowledge, this is the first report documenting the ability to detect time-dependent changes in FDG brain uptake at this temporal and spatial resolution.

For DREAMM experiments, we used herpes simplex virus (HSV) vectors expressing an engineered DREADD receptor under the control of the *Pdyn* or *Penk* promoter, which had been previously validated to drive selective expression of the inhibitory G_i-coupled hM_4Di DREADD in *Pdyn*- and *Penk*-MSNs (13) and whose specificity we also validated here (Figure 2, A and B). This strategy would thus allow, respectively, G_i-mediated inhibition of "Go," or activation of "NoGo" MSN output pathways (10). First, we assessed whether hM_4Di-mediated inhibition of NAcSh *Pdyn*- or *Penk* -MSNs reduced neuronal activity locally. Adult (P55–P69) male SD rats were infused into the right NAcSh with the *Pdyn*- or *Penk*-hM_4Di HSV constructs (n = 6/group) (Figure 2C). Two weeks later, rats received an i.p. injection of clozapine-n-oxide (CNO) (1 mg/kg), which promotes G_i-coupled inhibition of hM_4Di-expressing *Pdyn*- and *Penk*-MSNs (13), were sacrificed 1 hour later and processed for c-Fos immunohistochemistry. Consistent with prior reports in which G_i-mediated activation was associated with decreases in c-Fos (13, 14), we found that hM_4Di activation in NAcSh *Pdyn*-MSNs decreased c-Fos activation locally in the ipsilateral NAc as well as in the VTA (Figure 3). On the other hand, *Penk*-MSN inhibition decreased c-Fos activity only in the ipsilateral NAc, but not in VTA (Figure 3). These findings emphasize the specificity in neuronal inhibition achieved using DREADD.

Next, we attempted to detect in vivo the functional whole-brain dynamic circuits associated with inhibition of *Pdyn*- or *Penk*-MSNs. Male adult SD rats (n = 6/group) were infused into the right NAcSh with *Pdyn*- or *Penk*-hM_4Di constructs and scanned at 7 (after i.p. injection of vehicle) and 14 days (after i.p. CNO) after vector injection. Immediately after injection (vehicle or CNO), rats were anesthetized (1.5% isoflurane), injected i.v. with FDG (~0.6 mCi) and scanned using the above dynamic scanning methodology. All images were then normalized to Paxinos stereotaxic coordinates (12) and analyzed as previously described (7). Significant DREAMM responses in areas with direct, known connectivity of *Pdyn*- and *Penk*-MSNs were observed as early as 1 minute after scanning (Figure 4). In particular, *Pdyn*-MSN inhibition led to a significant increase in FDG uptake in areas coincident with the posterior VP and VTA/substantia nigra (SN) (Figure 4A), whereas *Penk*-MSN inhibition led to a significant decrease in FDG uptake in a cluster approximating the rostral VP (Figure 4B). Similar to the vibrissae stimulation model in which we observed time-dependent recruitment of barrel field circuits, *Pdyn*- and *Penk*-MSN inhibition resulted in discrete time-dependent DREAMM responses that spanned recruitment of specific brain regions and revealed distinct network patterns for each MSN subtype (Figure 4, A and B). In particular, *Pdyn*-MSN inhibition induced a time-dependent continuum of decreased FDG uptake throughout the ipsilateral ventral forebrain extending from the olfactory tubercle through the hypothalamus to the interpeduncular midbrain region and brainstem. This ventral inhibitory DREAMM circuit was coincident with a broad time-dependent increase in FDG uptake in the dorsal pallidum and midbrain followed by other dorsal structures extending from midline cingulate cortices (CG), throughout the dorsal hippocampus (HP) to the cerebellar nuclei (Figure 4A). In contrast, *Penk*-MSN inhibition was predominantly characterized

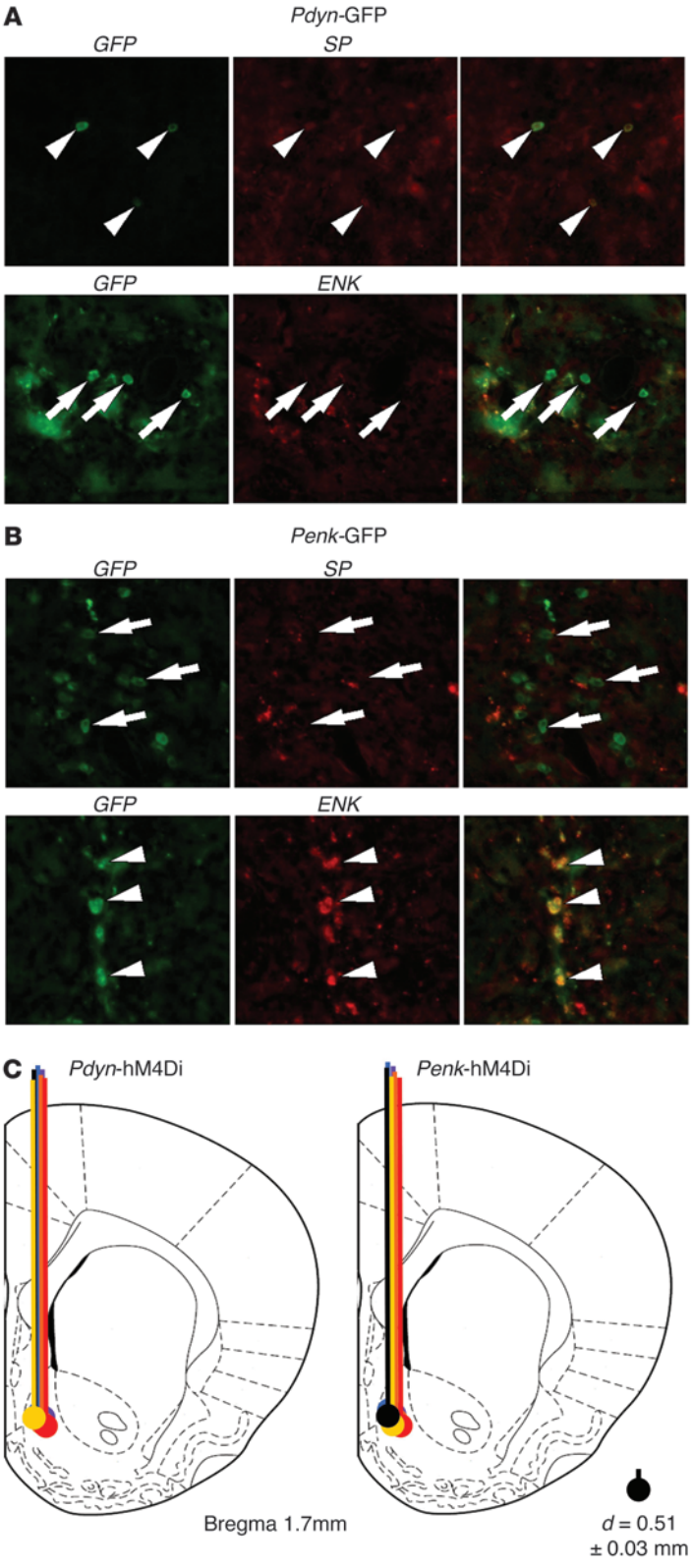

Figure 2
Validation of HSV vector selectivity and infusion sites. (**A**) Representative images from the NAc of rats injected with HSV-*Pdyn*-GFP (**A**) or HSV-*Penk*-GFP (**B**) and assessed for substance P (SP) (which coexpresses with *Pdyn* and not *Penk*) or enkephalin (Enk) immunoreactivity. In rats injected with *Pdyn*-GFP, 100% of cells were positive for both GFP and SP (arrowheads) and 4.5% were positive for GFP and Enk (arrows). In rats injected with *Penk*-GFP, we found that 6.7% of cells were positive for both GFP and SP (arrows) and 76.7% were positive for GFP and Enk (arrowheads). Original magnification, ×20. (**C**) Schematic image of injection sites and viral spread of HSV-*Pdyn*-hM$_4$Di and HSV-*Penk*-hM$_4$Di vectors. Mean diameter (d) of area surrounding each injection site was measured at 0.51 ± 0.03 mm (SEM).

by a time-dependent reduction of ipsilateral FDG uptake in the olfactory tubercle, VP, globus pallidus, ventral pons, sensory brainstem nuclei, and cerebellum as well as ipsilateral FDG increases in the dorsal HP, caudate putamen, and septofimbrial nucleus (Figure 4B). The more widespread effects of *Pdyn*-MSN inhibition as compared with *Penk*-MSN implicates a greater role of the "Go" pathway in modulating brain activity under anesthetized conditions.

To validate the specificity of DREAMM to discern FDG changes within discrete brain regions, nonbiased SPM results were also expressed quantitatively using a novel region of interest–based (ROI-based) image analysis method that used Paxinos stereotaxic rat coordinates to extract individual subject values for the VTA/SN. Using this approach, individual subject values plotted for the VTA/SN, which specifically dissociate *Pdyn* and *Penk* projections, revealed that, in agreement with SPM, inhibition of *Pdyn*-MSNs led to a significant increase (8.6%) in FDG uptake in the VTA/SN at 1 minute into the scan, whereas after 30 minutes, and consistent with both SPM and c-Fos results, CNO significantly decreased FDG uptake (7.2%) in this region (Figure 4C). Importantly, in agreement with a lack of direct anatomical connectivity with the VTA/SN, no significant differences were observed in this region at either 1 or 30 minutes in response to *Penk*-MSN inhibition (Figure 4D). Many studies have now shown convincingly that CNO does not have any off-target effects in a variety of experimental parameters in both rats and mice (13, 15–20). In order to expand this to brain and peripheral glucose metabolism, and since the transaxial field of view of the scanner did not accommodate whole-body rat scans, we scanned naive adult male mice (n = 6) twice, once after i.p. CNO (1 mg/kg) and once after i.p. vehicle injection. Consistent with numerous prior observations for a lack of off-target effects of CNO on behavior, neurophysiology, and pharmacology in both rats and mice, we did not observe any significant changes in FDG uptake between vehicle and CNO scans (Supplemental Figure 1; supplemental material available online with this article; doi:10.1172/JCI72117DS1). Overall, these results suggest that, in anesthetized rats, DREAMM is able to successfully capture cell-specific, time-dependent changes in brain functional activity with single-minute resolution.

Next, we assessed DREAMM functional connectivity of NAcSh *Pdyn*- and *Penk*-MSNs associated with FDG uptake in the awake state using a well-established behavioral imaging paradigm (6–9). Male adult SD rats (n = 6) were inject-

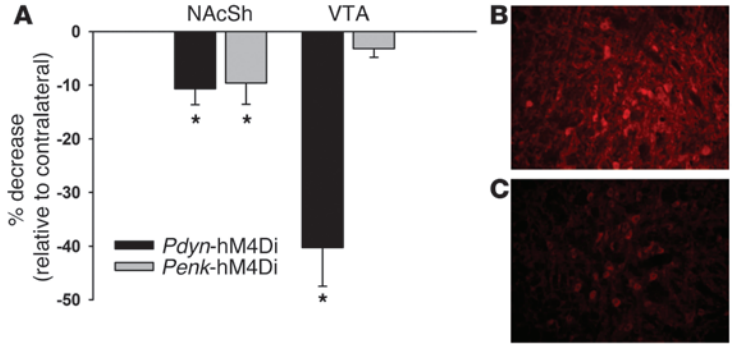

Figure 3
Cell-type–specific control of local and long-range signaling is detected using c-Fos immunostaining. (**A**) *Pdyn*-MSN inhibition decreased c-Fos in the ipsilateral NAcSh (~10%) and VTA (~40%), while *Penk*-MSN inhibition decreased c-Fos only in NAcSh (~10%) (n = 5/group). (**B** and **C**) Representative fluorescent microscopy images of contralateral (**B**) and ipsilateral (**C**) c-Fos fluorescence in the same brain section of the VTA. *P < 0.05. Data represent mean ± SEM. Original magnification, ×20.

ed i.p. with vehicle or CNO and placed in an open-field arena. At 30 minutes, rats were injected i.p. with FDG (~0.6 mCi), and 30 minutes subsequently, they were anesthetized and scanned for 20 minutes using a static acquisition protocol. We found that reducing neuronal activity of the right NAcSh *Pdyn*-MSNs significantly increased left turn motor behavior (P = 0.006) (Figure 5A), and this was paralleled by significant increases in counter-clockwise (leftward) circling (P = 0.001) (Figure 5B). Interestingly, *Pdyn*-MSN inhibition significantly increased (8.8%) FDG uptake in the right motor cortex (MC) (Figure 5C). Inhibition of *Penk*-MSNs significantly decreased FDG uptake in MC bilaterally, though this was more pronounced in the right MC (14.4%) (Figure 5F). In line with the DREAMM pattern, CNO increased ipsilateral (right) versus contralateral turns (P = 0.05) (Figure 5D), but there was no difference in general clockwise vs. counter-clockwise circling (Figure 5E). These findings are consistent with contralateral control of motor behavior by the MC and emphasize the ability of DREAMM to map behavior to global brain functional circuits of discrete yet spatially overlapping cell types. Paradoxically, the directionality in turning behaviors we currently observed after inhibition of direct and indirect pathway ventral striatal MSNs was similar to that previously reported by Kravitz et al. after activation of the dorsal MSN pathways (21). Interestingly, duration of stimulation may account for these findings, since acute and sustained inhibition led to time-dependent, opposing changes in FDG uptake in downstream projection sites. Such time-dependent changes in FDG uptake are likely mediated by changes in complex downstream signaling plasticity mechanisms relevant to spatiotemporal control of G_i signaling (22, 23).

Similar to what was found under anesthetized conditions, discrete DREAMM responses were observed following *Pdyn*- and *Penk*-MSN inhibition in freely moving rats that had distinct limbic-related profiles associated with each NAc pathway (Figure 6). *Pdyn*-MSN inhibition was associated with significant FDG uptake in ipsilateral corticolimbic circuits, including a striking 17.8% ipsilateral increase in the medial entorhinal cortex (Ent) and approximately 10%–12% alteration throughout the ipsilateral rostrocaudal extent of the VP and horizontal limb of the diagonal band (HDB) (Figure 6, A and B). There were also significant bilateral increases in medial amygdala (MEA) (13% ipsilateral; 4.8% contralateral) and retrosplenial cortex (12.3% ipsilateral; 9.8% contralateral). In addition, FDG uptake was increased in the entire contralateral rostrocaudal extent of the dysgranular insula (DI) (8.1%) and CG (8.2%). Overall, only increased FDG uptake was observed with NAcSh *Pdyn*-MSN inhibition, whereas both increased and decreased uptake were observed with *Penk*-MSN inhibition in the awake, moving rodent (Figure 6, C and D). Intriguingly, inhibiting *Penk*-MSN activity resulted in significant ipsilateral FDG increases in primary components of the limbic system including the VP (8.8%), amygdala (basal [14%] and medial [8.3%] divisions), and HP (8.6%) (pronounced demarcation of the dentate gyrus). Such HP and amygdala activation is particularly interesting, given recent studies demonstrating a role for the "indirect" NAcSh *Penk*-MSNs in mediating behavioral responses associated with aversive memory formation (24). Indeed, a unique feature of the *Penk*-MSN manipulation was increased FDG uptake (8.2%–11.3%) along the fornix, which primarily connects the HP with the septum and diencephalon. Interestingly, NAcSh *Penk*-MSN inhibition also led to a striking bilateral activation of the DI (14.6% ipsilateral and 17.3% contralateral), and ventromedial PFC, particularly the medial orbital area (12.4% ipsilateral and 12.5% contralateral). Finally, and in contrast to *Pdyn*-MSN inhibition, *Penk*-MSN inhibition led to significant decreases in FDG uptake in the ipsilateral sensory cortex (SC) (14.7%), globus pallidus (GP) (5.7%), and contralateral piriform cortex (Pir) (17.6%). Overall, these findings identify distinct neural activity associated with *Pdyn* and *Penk* limbic striatal pathways and emphasize that direct NAc pathway impairments have profound bottom-up regulation, particularly of limbic-related cortices. Additionally, the recruitment of motor systems (e.g., dorsal striatopallidal circuit and MC) by NAcSh *Penk*-MSN inhibition emphasizes the strong limbic-motor interface of this pathway.

Discussion

The DREAMM technique now adds to the growing number of research strategies in the neuroscience toolbox to assess in vivo brain function. Specifically, it provides, in contrast to other current techniques, the ability to measure in vivo time-dependent, regionally unbiased, whole-brain activity after cell-specific manipulations via a well-understood molecular process (glucose utilization). Importantly, while current imaging strategies have been limited to assessing brain function in immobilized animals, the unique kinetics of FDG allow time-dependent brain activity measures that occur during the awake, freely moving state. DREAMM is most suited for studying behavioral profiles generated from ensembles of neurons than those relevant to the activity of a single cell. Moreover, DREAMM does not rely on complex surgical practices (chronic indwelling cannulas), which induce significant decreases in brain activity and inflammatory responses as well as cognitive deficits (25, 26). Since DREAMM is not limited to probing cellular activity, it could also be used to provide insights into

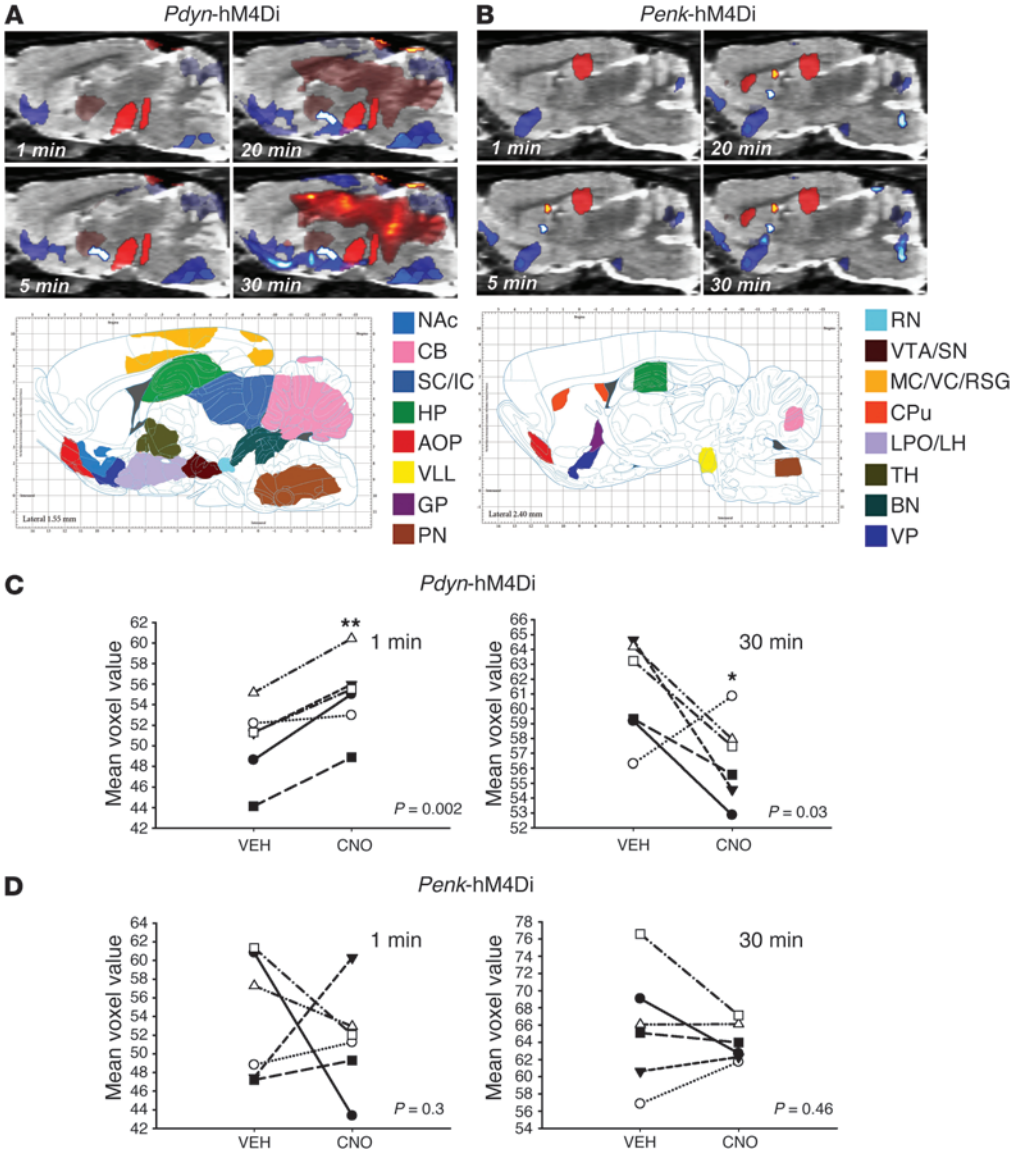

Figure 4
Cell-type–specific, time-dependent control of local and long range signaling is detected using DREAMM in anesthetized rats. Time-dependent DREAMM responses after (**A**) *Pdyn*- and (**B**) *Penk*-expressing MSN inhibition ($P = 0.05$; relative increase [red] and decrease [blue] in FDG uptake) in sagittal planes and corresponding images from the Paxinos rat brain atlas. Individual subject voxel values in the VTA showing that *Pdyn*-MSN inhibition significantly increases FDG uptake at 1 minute ($P = 0.002$) and decreases FDG uptake at 30 minutes ($P = 0.03$) (**C**) in comparison with vehicle condition, while *Penk*-MSN inhibition does not (**D**). CB, cerebellum; IC, inferior colliculus; AOP, anterior olfactory nucleus; VLL, ventral nucleus of lateral lemniscus; PN, pontine nuclei; RN, reticular nuclei; VC, visual cortex; RS, retrosplenial cortex; CPu, caudate putamen; LPO, lateral preoptic area; LH, lateral hypothalamus; TH, thalamus; BN, brainstem nuclei. $^{*}P < 0.05$; $^{**}P < 0.01$.

neurotransmitter dynamics (picomolar sensitivity) via the use of displaceable, positron-emitting radioligands (i.e., [^{11}C]raclopride).

Together, the findings illustrate the potential of DREAMM to quantitatively delineate (a) dynamic changes in discrete whole-brain neuronal circuits in vivo, even with single-minute resolution in anesthetized animals, and (b) cell-type–specific whole-brain neuronal circuits recruited during the awake state. Overall, DREAMM fills a technological niche providing unbiased, direct, quantitative, and longitudinal information of a well-understood measure of cellular activity (i.e., glucose utilization) to inform on whole-brain functional connectivity. DREAMM can thus be an important reverse-engineering research strategy to dissect in vivo–specific neuronal networks associated with normal and pathologic behavior.

Methods

Viral-mediated DREADD expression. Adult (P55–P69) male SD rats were obtained from Charles River Laboratories and housed on a reversed 12-hour dark/12-hour light cycle with food and water available ad libitum. All rats were stereotaxically injected with 2 μl (0.2 μl/min) of purified HSV vectors expressing a triple hemagglutinin (HA) epitope–tagged hM4Di gene (1567 Kb) under the control of the *PDYN* or *PENK* promoter. Both vectors were injected unilaterally (right hemisphere) into the medial shell of the nucleus accumbens (NAc) using the following coordinates (from bregma: anteroposterior (AP), 1.7; mediolateral (ML), 0.8; dorsoventral (DV), 7.2 mm.

Vibrissae stimulation and FDG μPET imaging. Six adult naive male SD rats were fasted overnight to attain consistency in blood glucose levels, as abnormal blood glucose levels interfere with FDG uptake (27). Rats were transported to the μPET facility several hours prior to the scan to ensure habituation to the environment. Rats were anesthetized using isoflurane (1.5%) and placed on an Inveon μPET scanner bed (Siemens Medical Solutions); the left lateral tail vein was catheterized. Vibrissae stimulation was immediately initiated (30 rpm) using a custom motorized stimulation device (always on the right side). Five minutes later, rats were injected i.v. with approximately 0.6 mCi of FDG and dynamic scan-

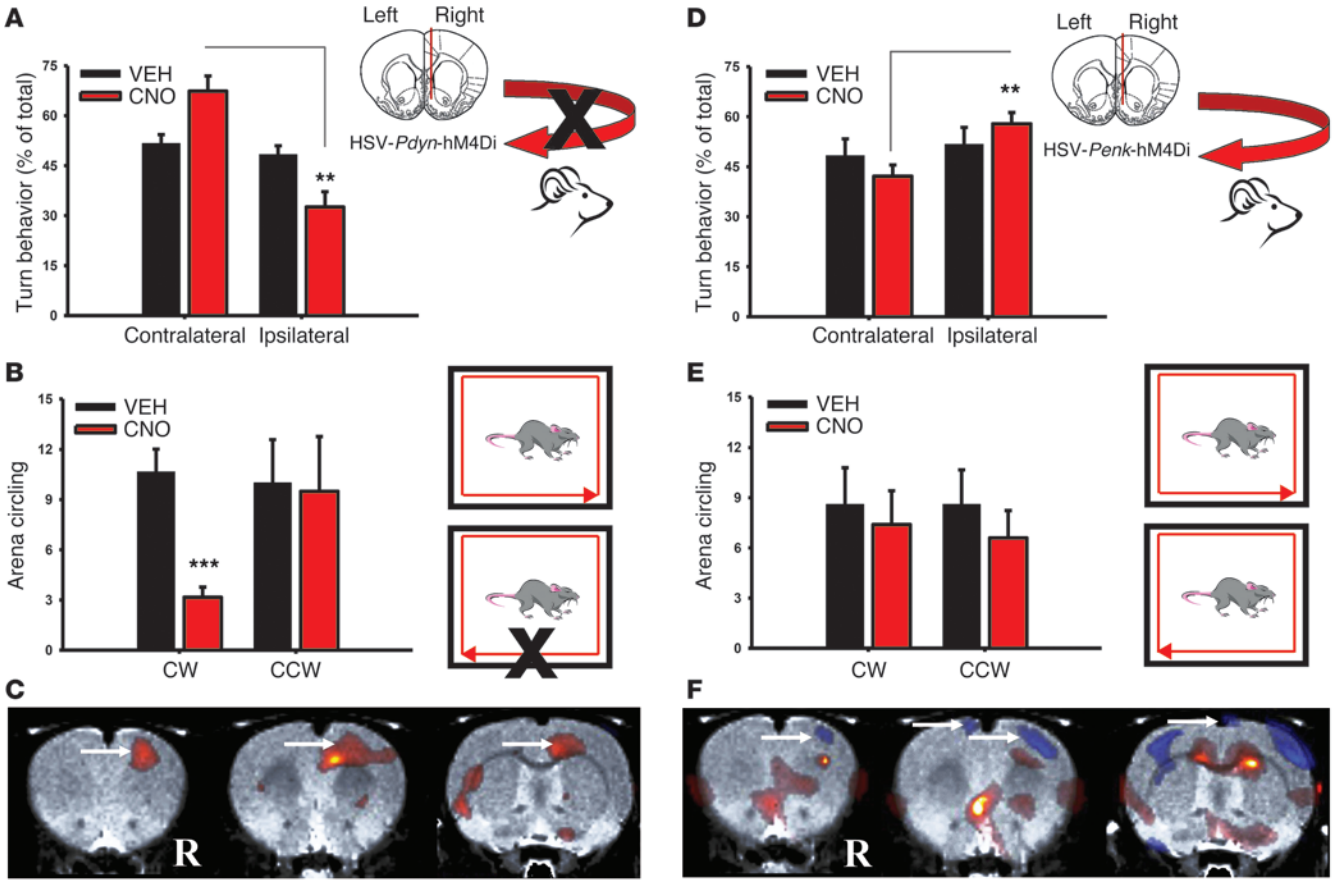

Figure 5

Unilateral inhibition of *Pdyn*- and *Penk*-expressing neurons in NAcSh leads to opposing patterns in turning behavior and MC activity. *Pdyn*-MSN inhibition (n = 6) increased contralateral turning (P = 0.006) (**A**) and significantly increased counter-clockwise (CCW) circling (P < 0.001) (**B**) CW, clockwise. *Pdyn*-MSN inhibition (n = 6) increased FDG uptake in the ipsilateral (right [R]) MC (arrows) (P = 0.05) (**C**). *Penk*-MSN inhibition (n = 5) increased ipsilateral turning (P = 0.01) (**D**), but did not significantly affect circling (**E**). *Penk*-MSN inhibition (n = 5) decreased FDG uptake in ipsilateral MC (arrows) (P = 0.05) (**F**). Data represent mean ± SEM. **P < 0.01; ***P < 0.001.

ning immediately commenced. Scans were histogrammed into 1-minute bins and reconstructed using the OSEM2D algorithm. Images were then processed and coregistered to an MRI stereotaxic atlas. Coregistered images were then flipped along the horizontal axis for each subject. These images were then compared using SPM, allowing us to conduct interhemispheric comparisons.

In vivo DREAMM in behaving rats. Rats were transported to the μPET facility the day prior to each scan to ensure habituation to the transportation procedure and environment. All rats were then fasted overnight to attain consistency in blood glucose levels, as abnormal blood glucose levels interfere with FDG uptake (27). The next day, rats received an i.p. injection of either vehicle (day 7 after vector injection) or the DREADD-activating ligand CNO (day 14 after vector injection) (1 mg/kg). Immediately after vehicle or CNO injection, rats were anesthetized with isoflurane (1.5%), placed in a prone position on the bed of an R4 microPET rodent scanner (Siemens Medical Solutions), and injected i.v. with FDG (~0.6 mCi). Scanning was initiated concurrently with FDG injection, and each scan lasted for 30 minutes and was acquired using a dynamic protocol. For behavioral imaging experiments, each rat was injected i.p. with either vehicle (day 9 after vector injection) or CNO (1 mg/kg) (day 16 after vector injection) and immediately placed in an open-field arena (40.64 × 40.64 × 40.64 cm) coupled to an activity monitoring system (Truscan; Coulbourn Instruments) and a video recording device. Thirty minutes later, data collection was paused and each rat was injected i.p. with FDG (~0.6 mCi) and placed back into the arena, with data collection resuming for another 30 minutes (60 minutes total). Rats were then anesthetized with isoflurane (1.5%) and scanned for 20 minutes using a static acquisition protocol. For mouse experiments, we used 6 naive adult C57BL/6 male mice, which were scanned twice, once with vehicle and once with CNO (1 mg/kg). Mice were transported to the facility the day before the scans and fasted overnight. They were injected with either vehicle or CNO (1 mg/kg) and 15 minutes later injected i.p. with approximately 0.2 mCi FDG and placed in their home cage for a 30-minute tracer uptake period. Afterwards, mice were anesthetized with isoflurane (1.5%) and scanned for 20 minutes as above. All images were reconstructed using the maximum a posteriori (MAP) algorithm, as previously described (8). After reconstruction, images were spatially processed and normalized using the Pixel-Wise Modeling Software Suite (PMOD; PMOD Inc.) to a rat brain MRI template set to Paxinos and Watson stereotaxic coordinates (12). Constraining the reconstruction of the metabolic images into MRI-derived neuroanatomical templates significantly

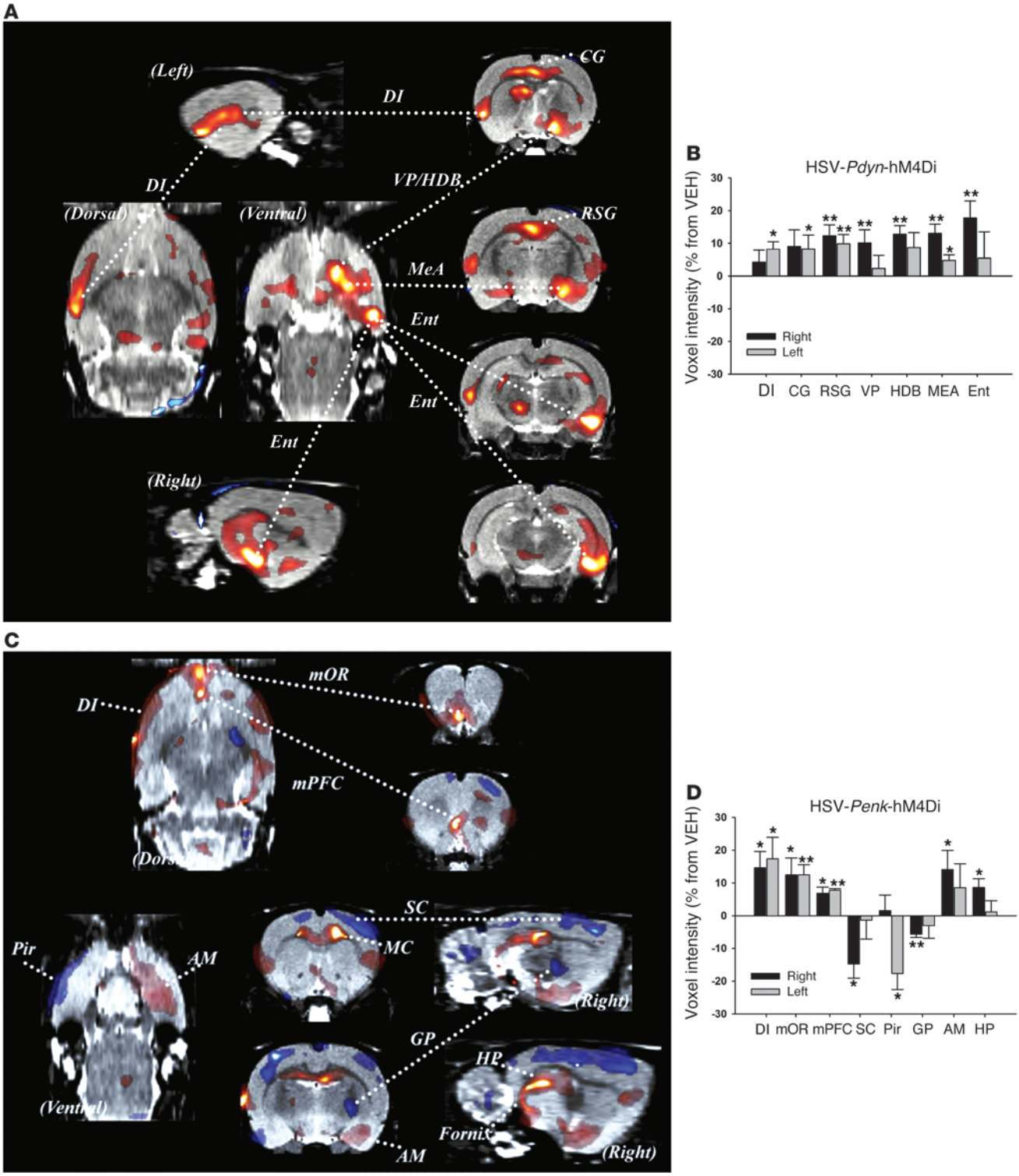

Figure 6

Unilateral inhibition of spatially overlapping *Pdyn- and Penk*-expressing neurons in NAcSh of freely moving rats leads to changes in distinct neural circuits. (**A**) *Pdyn*-MSN inhibition ($n = 6$) increased FDG uptake in specific corticolimbic regions including the Ent, DI, CG, and MEA as well as VP/HDB as visualized in coronal, sagittal and horizontal planes and (**B**) as plotted as percentage change in signal response $^{*}P < 0.05$; $^{**}P < 0.01$. (**C**) *Penk*-MSN inhibition ($n = 5$) led to profound activation of the DI, medial orbital prefrontal cortices (mOR and mPFC), HP circuit, amygdala, VP, and decreased activity of SC, and Pir, and GP, as visualized in coronal, sagittal and horizontal planes and (**D**) as plotted as percentage change in signal response. $^{*}P < 0.05$; $^{**}P < 0.01$. Data represent mean ± SEM.

improves both the sensitivity and anatomical specificity to detect alterations in FDG uptake using SPM (28, 29). As such, normalized scans were then analyzed as previously described (7). All SPM contrasts consisted of paired *t*-tests within each group (e.g., vehicle > CNO, vehicle < CNO) and were evaluated at the uncorrected $P = 0.05$ level as per our a priori hypotheses. Only clusters of at least 100 contiguous voxels were reported. For quantitative analysis of regional SPM differences we modified an SPM ROI toolbox (MarsBaR v0.43) for use with our rat stereotaxic MRI atlas. Stereotaxic coordinates were entered into MarsBaR for the desired brain areas, which allowed the extraction of individual subject data for each stereotaxically defined brain area. For behavioral data, we used the videotaped sessions to calculate the number of right or left 90° turns each rat made during the open-field experiments. In addition, data collected with the Truscan system were also analyzed. All comparisons were assessed for significance using paired *t* tests ($P = 0.05$).

DREADD expression validation. Rats (Long Evans, 475–550 g at time of surgery) were anesthetized with 1.5%–3% isoflurane and received infusions of HSV vectors into NAc using the following coordinates: AP + 1.2, ML ± 2.0, DV –6.6. *Penk*-GFP and *Pdyn*-GFP (2 μl) were infused into opposite sides of each rat as previously described (13). After 12–14 days of recovery the rats were transcardially perfused with 4% paraformaldehyde (PFA) after deep pentobarbital anesthesia (100 mg/kg i.p.) and the brains were processed for immunohistochemistry. Floating sections (40 μm) were permeabilized in 0.5% Triton-X/PBS for 1 hour, then blocked in 5% normal goat serum (NGS)–0.25% Triton-X 100/PBS for 2 hours. Sections were then incubated in 2.5% NGS–0.25% Triton-X 100/PBS containing antibodies to substance P (1:400; AB1566, Chemicon/Millipore) or GFP (1:400; MAB3580, Chemicon/Millipore), and/or in PBS containing anti-methionine enkephalin antibodies (1:100; no. 20065, Immunostar); sections were incubated with gentle agitation at 4°C for 72 hours. Next, sections were rinsed 3 times in PBS and incubated in species-appropriate Alexa Fluor 488–conjugated (green) and/or Alexa Fluor 568–conjugated (red) goat secondary antibodies (1:500; Invitrogen) for 2 hours. Sections were washed 3 times in PBS, mounted on slides, and coverslipped with ProLong Gold mounting medium with DAPI (Life Technologies). Images were captured with a Zeiss AxioImager.M2 (Carl Zeiss AG) using the Zeiss ApoTome 2 for optical sectioning, with a ×20 (air) or ×40 (oil immersion) lens.

c-Fos and HA-tag immunostaining. Rats injected with *Pdyn*-hM$_4$Di and *Penk*-hM$_4$Di into NAcSh were injected i.p. with CNO (1 mg/kg) and perfused 1 hour later with 4% PFA. Brains were removed from the skull, postfixed in 4% PFA at 4°C overnight, and then cryoprotected in 30% sucrose. Floating brain sections (40 μm) were first washed in a solution of 0.5% Triton X-100, 1× PBS for 30 minutes at room temperature (RT). Sections were then transferred to a blocking solution of 5% NGS, 0.25% Triton X-100/1× PBS for 1 hour at RT. Primary antibodies for c-Fos (1:400; no. SC-52, Santa Cruz Biotechnology Inc.) or HA-tag (no. AB3254; Millipore) were added to the blocking solution and incubated 12–40 hours at 4°C. Sections were then washed 4 times in 0.4% Triton X-100/1× PBS solution and subsequently incubated with Alexa Fluor 568–conjugated (red) secondary antibodies (1:400; Invitrogen) in blocking solution for 1–2 hours. After incubation, sections were washed in 0.4% Triton X-100/1× PBS solution, mounted on slides, and coverslipped with Vectashield Hard Set Mounting Medium containing DAPI (Vectorlabs). Images were captured with the MVX10 Stereoscope (Olympus) using the MicroSuite Biological Suite 3.1 and fluorescence complimentary to the red diode (c-Fos) and 405 diode (DAPI). Images were also captured using the ArcturusXT (Applied Biosystems) microscope. ROIs encompassing the ipsilateral and contralateral NAcSh and VTA were analyzed ($n = 4–5$/group) using ImageJ v1.45 software (NIH).

It is important to note that inconsistencies between DREAMM and c-Fos are expected as FDG is a direct marker of brain activity (i.e., glucose metabolism) and is thought to predominantly label terminals (presynaptic activity), whereas c-Fos is a transcription factor and correlational marker of postsynaptic activity (cell body). In addition, DREAMM differences are represented as statistical estimations of effect size between 2 different conditions (vehicle vs. CNO) for a single subject whereas differences in c-Fos immunostaining reflect interhemispheric differences (DREADD vs. control) during the CNO condition. Finally, differences in temporal expression of c-Fos (limited to 60–90 minutes after stimulus) also limit direct comparisons between these 2 measures. In sum, DREAMM is difficult to compare to in vitro measures, as the main premise is that it allows one to obtain data from awake, freely moving animals, thus having each animal serve as its own control.

Statistics. Imaging analysis was performed using SPM8. This approach relies on using the general linear model and applying a statistical threshold to all voxels for all scans. Only clusters comprising with a *P* value of less than 0.05 were reported. Additionally, in an effort to limit false positives, we only reported significant clusters comprising of greater than 100 contiguous voxels as previously described (7, 8). The maps surviving the $P = 0.05$ threshold were then analyzed using paired *t* tests (vehicle > CNO and vehicle < CNO for the groups: *Pdyn*-hM$_4$Di, *Penk*-hM$_4$Di, C57BL/6 mice) and (left hemisphere vs. right hemisphere for the rats used in the vibrissae stimulation experiment). This approach is analogous to ANOVA followed by pair-wise comparisons and is a standard in the field, since it takes into consideration that both measures are obtained from the same animal. Also, this specific approach has been validated previously by directly comparing in vivo FDG-PET with ex vivo FDG-autoradiography in rats (30). Since SPM is limited to just visualizing the maps that survived the significance analysis, we subsequently extracted individual data from significant clusters of each scan using a ROI approach. Behavioral data was analyzed using ANOVA with repeated measures within each session and paired *t* tests to determine group differences (i.e., *Pdyn*-hM$_4$Di and *Penk*-hM$_4$Di under vehicle and CNO conditions). Finally, ipsilateral vs. contralateral c-Fos activation data were statistically compared using paired *t* tests. All tests were evaluated at $P < 0.05$.

Study approval. All animal experiments were approved by the Brookhaven National Laboratory and University of Washington animal care and use committees and were conducted in accordance with the NIH Guide for the care and use of laboratory animals.

Acknowledgments

This work was supported by the National Institute on Alcohol Abuse and Alcoholism (NIAAA) (AA11034, AA07574, and AA07611) and the National Institute on Drug Abuse (NIDA) (DA015446, DA023214, and DA030359). M. Michaelides was supported by the NIDA Postdoctoral Training Program at MSSM (DA007135). The authors thank the Mount Sinai Microscopy Shared Resource Facility and the microPET Facility (Wade Koba, Linda Jelicks) at the Albert Einstein College of Medicine of Yeshiva University.

Received for publication July 15, 2013, and accepted in revised form September 12, 2013.

Address correspondence to: Yasmin L. Hurd, Icahn School of Medicine at Mount Sinai, Hess Center for Science and Medicine, 10th Floor Room 105, 1470 Madison Avenue, New York, New York 10029, USA. Phone: 212.824.9313; Fax: 646.537.9598; E-mail: yasmin.hurd@mssm.edu.

1. Lee JH, et al. Global and local fMRI signals driven by neurons defined optogenetically by type and wiring. *Nature*. 2010;465(7299):788–792.
2. Desai M, et al. Mapping brain networks in awake mice using combined optical neural control and fMRI. *J Neurophysiol*. 2011;105(3):1393–1405.
3. Christie IN, et al. fMRI response to blue light delivery in the naive brain: Implications for combined optogenetic fMRI studies. *Neuroimage*. 2012; 66C:634–641.
4. Armbruster BN, Li X, Pausch MH, Herlitze S, Roth BL. Evolving the lock to fit the key to create a family of G protein-coupled receptors potently activated by an inert ligand. *Proc Natl Acad Sci U S A*. 2007; 104(12):5163–5168.
5. Rogan SC, Roth BL. Remote control of neuronal signaling. *Pharmacol Rev*. 2011;63(2):291–315.
6. Michaelides M, Thanos PK, Volkow ND, Wang GJ. Translational neuroimaging in drug addiction and obesity. *ILAR J*. 2012;53(1):59–68.
7. Michaelides M, et al. Dopamine D4 receptors modulate brain metabolic activity in the prefrontal cortex and cerebellum at rest and in response to methylphenidate. *Eur J Neurosci*. 2010;32(4):668–676.
8. Thanos PK, et al. Differences in response to food stimuli in a rat model of obesity: in-vivo assessment of brain glucose metabolism. *Int J Obes (Lond)*. 2008; 32(7):1171–1179.
9. Aarons AR, Talan A, Schiffer WK. Experimental protocols for behavioral imaging: seeing animal models of drug abuse in a new light. *Curr Top Behav Neurosci*. 2012;11:93–115.
10. Zhou L, Furuta T, Kaneko T. Chemical organization of projection neurons in the rat accumbens nucleus and olfactory tubercle. *Neuroscience*. 2003; 120(3):783–798.
11. Miyashita E, Keller A, Asanuma H. Input-output organization of the rat vibrissal motor cortex. *Exp Brain Res*. 1994;99(2):223–232.
12. Schweinhardt P, Fransson P, Olson L, Spenger C, Andersson JL. A template for spatial normalisation of MR images of the rat brain. *J Neurosci Methods*. 2003; 129(2):105–113.
13. Ferguson SM, et al. Transient neuronal inhibition reveals opposing roles of indirect and direct pathways in sensitization. *Nat Neurosci*. 2011; 14(1):22–24.
14. Le Moine C, Svenningsson P, Fredholm BB, Bloch B. Dopamine-adenosine interactions in the striatum and the globus pallidus: inhibition of striatopallidal neurons through either D2 or A2A receptors enhances D1 receptor-mediated effects on c-fos expression. *J Neurosci*. 1997;17(20):8038–8048.
15. Abdul-Ridha A, Lane JR, Sexton PM, Canals M, Christopoulos A. Allosteric modulation of a chemogenetically modified G protein-coupled receptor. *Mol Pharmacol*. 2013;83(2):521–530.
16. Farrell MS, et al. A Galphas DREADD mouse for selective modulation of cAMP production in striatopallidal neurons. *Neuropsychopharmacology*. 2013; 38(5):854–862.
17. Garner AR, et al. Generation of a synthetic memory trace. *Science*. 2012;335(6075):1513–1516.
18. Krashes MJ, et al. Rapid, reversible activation of AgRP neurons drives feeding behavior in mice. *J Clin Invest*. 2011;121(4):1424–1428.
19. Zhan C, et al. Acute and long-term suppression of feeding behavior by POMC neurons in the brainstem and hypothalamus, respectively. *J Neurosci*. 2013; 33(8):3624–3632.
20. Sasaki K, Suzuki M, Mieda M, Tsujino N, Roth B, Sakurai T. Pharmacogenetic modulation of orexin neurons alters sleep/wakefulness states in mice. *PLoS One*. 2011;6(5):e20360.
21. Kravitz AV, et al. Regulation of parkinsonian motor behaviours by optogenetic control of basal ganglia circuitry. *Nature*. 2010;466(7306):622–626.
22. Pertz O. Spatio-temporal Rho GTPase signaling - where are we now? *J Cell Sci*. 2010;123(pt 11): 1841–1850.
23. Goldsmith ZG, Dhanasekaran DN. G protein regulation of MAPK networks. *Oncogene*. 2007; 26(22):3122–3142.
24. Hikida T, Kimura K, Wada N, Funabiki K, Nakanishi S. Distinct roles of synaptic transmission in direct and indirect striatal pathways to reward and aversive behavior. *Neuron*. 2010;66(6):896–907.
25. Frumberg DB, Fernando MS, Lee DE, Biegon A, Schiffer WK. Metabolic and behavioral deficits following a routine surgical procedure in rats. *Brain Res*. 2007;1144:209–218.
26. Schiffer WK, Mirrione MM, Biegon A, Alexoff DL, Patel V, Dewey SL. Serial microPET measures of the metabolic reaction to a microdialysis probe implant. *J Neurosci Methods*. 2006;155(2):272–284.
27. Wong KP, Sha W, Zhang X, Huang SC. Effects of administration route, dietary condition, and blood glucose level on kinetics and uptake of 18F-FDG in mice. *J Nucl Med*. 2011;52(5):800–807.
28. Gispert JD, et al. Influence of the normalization template on the outcome of statistical parametric mapping of PET scans. *Neuroimage*. 2003; 19(3):601–612.
29. Gutierrez D, et al. Anatomically guided voxel-based partial volume effect correction in brain PET: impact of MRI segmentation. *Comput Med Imaging Graph*. 2012;36(8):610–619.
30. Prieto E, et al. Statistical parametric maps of ^{18}F-FDG PET and 3-D autoradiography in the rat brain: a cross-validation study. *Eur J Nucl Med Mol Imaging*. 2011;38(12):2228–2237.